



# MODELICA

Proceedings  
of the 4th International Modelica Conference,  
Hamburg, March 7-8, 2005,  
Gerhard Schmitz (editor)

T. Hirsch, W. Steinmann, M. Eck  
*DLR Stuttgart, Germany*

**Simulation of transient two-phase flow in parabolic trough collectors using Modelica**

pp. 403-412

Paper presented at the 4th International Modelica Conference, March 7-8, 2005, Hamburg University of Technology, Hamburg-Harburg, Germany, organized by The Modelica Association and the Department of Thermodynamics, Hamburg University of Technology

All papers of this conference can be downloaded from  
<http://www.Modelica.org/events/Conference2005/>

#### Program Committee

- Prof. Gerhard Schmitz, Hamburg University of Technology, Germany (Program chair).
- Prof. Bernhard Bachmann, University of Applied Sciences Bielefeld, Germany.
- Dr. Francesco Casella, Politecnico di Milano, Italy.
- Dr. Hilding Elmqvist, Dynasim AB, Sweden.
- Prof. Peter Fritzson, University of Linkping, Sweden
- Prof. Martin Otter, DLR, Germany
- Dr. Michael Tiller, Ford Motor Company, USA
- Dr. Hubertus Tummescheit, Scynamics HB, Sweden

Local Organization: Gerhard Schmitz, Katrin Pröhl, Wilson Casas, Henning Knigge, Jens Vassel, Stefan Wischhusen, TuTech Innovation GmbH

# Simulation of transient two-phase flow in parabolic trough collectors using Modelica

Dipl.-Ing. Tobias Hirsch   Dr.-Ing. Markus Eck   Dr.-Ing. Wolf-Dieter Steinmann  
German Aerospace Center, Institute of Technical Thermodynamics  
Pfaffenwaldring 38-40, 70569 Stuttgart

## Abstract

Parabolic trough power plants are a very promising option for the generation of electricity from renewable energy resources. The Modelica library 'DissDyn' is developed to study the transient behaviour of the two-phase flow inside the absorber tubes of such plants. Equations are based on a homogeneous equilibrium model for the pipe flow with axial discretization. The advantages of manually transforming the equations into explicit state space form are shown. The models are validated with analytical solutions and measured data. Using test signals for disturbances in solar irradiation important information on the liquid loads on field separator and drainage system are gained. By adding feed-forward control schemes it is shown that these loads can be reduced significantly.

*Keywords:* solar thermal power plant; two-phase flow; simulation; renewable energy; absorber tube

## 1 Introduction

One way of generating electricity from renewable energy resources is the collection of solar radiation to be used in solar thermal power plants. Today's only commercially operated solar power plants in the Mojave Desert in California are based on a parabolic trough collector field. A synthetic oil is heated in the absorber tube and generates steam of 10 MPa/370°C in a heat exchanger unit. The steam is used to run a conventional steam turbine. Current research activities [1] are dealing with the direct solar steam (DISS) generation in the absorber tube itself. Improvements are expected by omitting the heat exchanger unit and allowing for higher steam temperatures thus leading to an increase in turbine efficiency. To avoid material problems caused by an undefined end of the evaporation section the collector loop is divided into two sections, see fig. 1. The evaporation section is run with a water surplus which has to be separated

from the steam before the entrance into the superheating section. In the current design realized at a DISS test loop in Almeria (Spain) a maximum of 1.2 kg/s of superheated steam at 3 to 10 MPa and 400°C is obtained from one collector loop. For the first pre-commercial power plant with this technology the dynamic behaviour of the system determines the design of key components like compact field separators and the underlying drainage system. A dynamical simulation tool based on the Modelica language is developed to study the effect of irradiation disturbances and to evaluate different control strategies. For the assembly of the final system and the numerical integration the Dymola program is used.

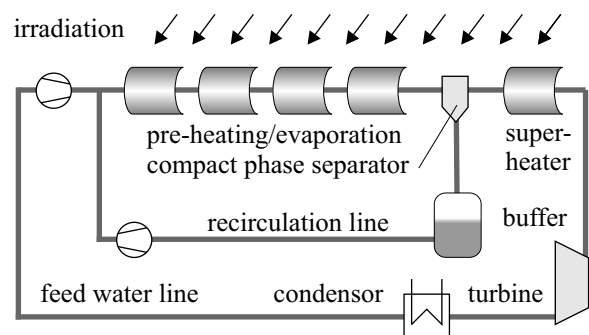


Figure 1: Configuration of a parabolic trough solar power plant with direct steam generation

## 2 Two-phase flow model equations

The central part of the model library is the fluid dynamical model of the two-phase flow in the absorber pipes. In the following the underlying assumptions and model equations are presented. For complex models it is advantageous and in this case necessary that the selection of state variables is done by the programmer and not by the symbolic transformation tool Dymola. It is shown that the combination of pressure and specific enthalpy is the best choice for the state vari-

ables of the fluid elements. The benefits of this manual selection of states and transformation of equations are

- stable and numerically efficient simulation
- independence of system assembly
- reliable initialization procedure
- well defined closure equations.

## 2.1 Conservation equations

Depending on the location along the collector loop different flow regimes are found in the absorber tube. Starting with single-phase liquid flow in the preheating part the flow changes into two-phase flow as soon as saturation conditions are reached. In the superheating section the flow is again single-phase. Superheating conditions also occur in the evaporator section when the end of the evaporation section dries out due to irradiation transients. Therefore the simulation model must be able to simulate the flow in the three regimes but also the transition between them. With a length of about 1000 m pressure losses in each loop are significant. Fluctuations in irradiation cause large changes in mass flow and, as a consequence, in absolute pressure in the field. For this reason it is necessary to use pressure-dependent properties for the fluid. It is assumed that the flow is homogeneous over the pipe cross-section. In the two-phase region equal velocities and temperatures of water and steam phase are assumed (homogeneous equilibrium model). The simulation model is intended to study effects resulting from mass and energy transport which are much slower than the propagation of changes in pressure. Therefore infinite velocity of propagation is assumed for the pressure. This reduces the momentum equation to a stationary momentum balance for frictional pressure losses. The fundamental equations for conservation of mass, energy and momentum for the control volume shown in fig. 2.1 thus yield

$$\frac{\partial \rho}{\partial t} + \frac{\partial}{\partial z}(\rho w) = 0 \quad (1)$$

$$\frac{\partial}{\partial t}(\rho u) + \frac{\partial}{\partial z}(\rho w h) = \frac{\dot{Q}}{V} \quad (2)$$

$$\frac{\partial p}{\partial z} = \Delta p \quad (3)$$

The system is completed by the energy equation

$$A_W \rho_W c_W \frac{T_W}{\partial t} = \dot{Q}_{\text{ext}} - \dot{Q} \quad (4)$$

for the surrounding pipe wall.

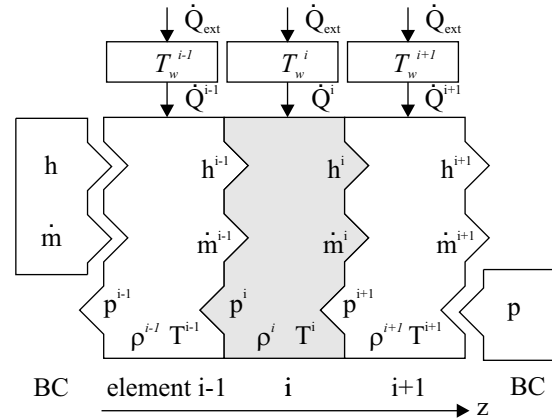


Figure 2: Three control volumes for pipe flow.

## 2.2 Selection of states

Two variables are sufficient to fully describe the state of the fluid element. The careful choice of the state variables is of essential importance since it determines the structure of the final system of equations. For this work the state variables pressure  $p$  and specific enthalpy  $h$  are chosen for the following reasons. All fluid properties can be expressed as a polynomial function of  $p$  and  $h$ . Using temperature  $T$  instead of  $h$  is not possible since temperature and pressure are directly linked in the two-phase region. The steam fraction  $x$  can not be used since it is not defined in the single phase regions. Friction losses cause a conversion of mechanical into thermal energy while the sum of both  $h = u + p/\rho$  stays the same. By using specific enthalpy as a state, pressure loss terms can easily be defined by just changing the pressure and leaving  $h$  constant. The most important advantage of this selection is that spatially discretized systems will result in a set of de-coupled equations while a choice of e.g. mass flows and specific enthalpy leads to a coupled system. Using the fluid property functions

$$\rho = \rho(p, h) \quad (5)$$

$$u = u(p, h) \quad (6)$$

and average fluid velocity

$$w = \frac{\dot{m}}{0.25 \pi d^2 \rho} \quad (7)$$

the system of equations (1) to (2) can be rewritten explicit in the time derivatives

$$\frac{\partial h}{\partial t} = f_h(h, p, \dot{Q}, \dot{m}) \quad (8)$$

$$\frac{\partial p}{\partial t} = f_p(h, p, \dot{Q}, \dot{m}) \quad (9)$$

From these equations explicit state space form can be obtained by replacing  $\dot{m}$  with an inverse pressure loss relation and  $\dot{Q}$  with a correlation for heat transfer.

### 2.3 Fluid properties

Properties of fluids are defined for three regions, namely single phase water (region 1), two-phase water-steam (2) and single-phase steam (3) in the range  $3 \text{ MPa} < p < 12 \text{ MPa}$  and  $100 \text{ }^\circ\text{C} < T < 500 \text{ }^\circ\text{C}$ . Since state variables  $p$  and  $h$  are pre-selected all properties can be expressed as polynomial function of these variables. In the two-phase region the steam fraction  $x$  is defined as

$$x = \frac{h - h'}{h'' - h'} \quad (10)$$

with the specific enthalpies at saturation implemented in polynomial form

$$h'(p) = a_0 + a_1 p + a_2 p^2 + a_3 p^3 \quad (11)$$

$$h''(p) = A_0 + A_1 p + A_2 p^2 \quad (12)$$

The density in liquid and gas phase is approximated by polynomials of pressure and enthalpy

$$\rho_l(p, h) = b_0(p) + b_1(p)h + \dots + b_n(p)h^n \quad (13)$$

$$\rho_g(p, h) = B_0(p) + B_1(p)h + \dots + B_n(p)h^n \quad (14)$$

with the coefficients

$$b_i(p) = b_{i,1} + b_{i,2}p + \dots + b_{i,m}p^m \quad (15)$$

$$B_i(p) = B_{i,1} + B_{i,2}p + \dots + B_{i,m}p^m \quad (16)$$

Note that for the homogeneous model the steam fraction  $x$  based on the control volume is the same as the steam quality  $\dot{x}$  based on the mass flows of the two phases. The mixture density in the two-phase region is then given by

$$\rho(p, h) = \left( \frac{1}{\rho'} + x \left( \frac{1}{\rho''} - \frac{1}{\rho'} \right) \right)^{-1} \quad (17)$$

$$\rho' = \rho_l(p, h'(p)) \quad (18)$$

$$\rho'' = \rho_g(p, h''(p)) \quad (19)$$

This approach guarantees a continuous transition between the three regions. The calculation of temperature as function of pressure and enthalpy requires that for a fixed pressure exactly the same temperature is obtained when approaching the saturation line from the liquid region and the gas region. For this reason polynomial approximations are set up relativ to saturation conditions,

$$T_1(p, h) = T' + c_0(p) + c_1(p)(h - h') + \dots \quad (20)$$

$$T_g(p, h) = T' + C_0(p) + C_1(p)(h - h'') + \dots \quad (21)$$

For the calculation of the saturation temperature Antoine's law

$$T' = \frac{T_B}{(T_A - \log_{10}(\frac{p}{100}))} - T_C \quad (22)$$

with the constants  $T_A = 8.1$ ,  $T_B = 1656.39$ ,  $T_C = 223.2$  is used.

To complete the set of fluid property functions polynomial approximations for the dynamic viscosity, specific heat capacity, heat conductivity and surface tension have been derived for both phases. These quantities are needed for the calculation of pressure losses, and heat transfer coefficients. Table 1 gives an overview on the order of the polynomials and the accuracy achieved. High accuracy is desired for saturation enthalpies to reduce the errors in calculating very small steam fractions.

Table 1: Polynomial order of property functions and accuracy in the range 3...11 MPa, 500...3500 kJ/kg

Variable	Order in p	Order in h	Rel. error
$h'$	3		0.2%
$h''$	3		0.02%
$\rho_l$	3	2	2%
$\rho_g$	2	3	0.5%
$\eta_l$	2	4	1%
$\eta_g$	1	2	1%
$\lambda_l$	2	3	1%
$\lambda_g$	2	3	1%
$c_{p,l}$	2	3	1%
$c_{p,g}$	2	4	1%
$T_1$	1	3	0.5%
$T_g$	3	3	0.5%
$\sigma(T')$	3		1%

### 2.4 Spatial discretisation

Regarding the whole collector loop, mass flow and specific enthalpy at the inlet and pressure at the outlet are given as boundary conditions. For the spatial discretization of equations (8) and (9) an upwind scheme is applied for mass flow and specific enthalpy. Pressure losses are concentrated downstream of the control volume. Thus the equations yield for control volume  $i$

$$\frac{\partial h^i}{\partial t} = f_h(h^i, h^{i-1}, p^i, \dot{Q}^i, \dot{m}^i, \dot{m}^{i-1}) \quad (23)$$

$$\frac{\partial p^i}{\partial t} = f_p(h^i, h^{i-1}, p^i, \dot{Q}^i, \dot{m}^i, \dot{m}^{i-1}) \quad (24)$$

## 2.5 Pressure loss

The mass flow terms in equations (23) and (24) have to be expressed as function of the state variables. This is realized by the inverse pressure loss relation

$$\dot{m}^i = \dot{m}^i(p^i, p^{i+1}, h^i) \quad (25)$$

To avoid implicit equations a pressure loss correlation which can be solved analytically for  $\dot{m}$  is used [2].

## 2.6 Heat transfer

The heat flux  $\dot{Q}$  between wall and fluid is defined with the wall temperature  $T_W$  and the fluid temperature  $T$  in control volume  $i$

$$\dot{Q}^i = \alpha^i \pi d l (T_W^i - T^i) \quad (26)$$

The heat transfer coefficient  $\alpha$  can be calculated in terms of the state variables

$$\alpha^i = \alpha^i(h^i, p^i, \dot{m}^i) \quad (27)$$

with  $\dot{m}^i$  given in equation (25).

Replacing mass flow and heat flow terms in equations (23) and (24) the final simulation equations in explicit state space formulation are obtained

$$\frac{\partial h^i}{\partial t} = f_h(h^i, h^{i-1}, p^i, p^{i-1}, p^{i+1}, T_W^i) \quad (28)$$

$$\frac{\partial p^i}{\partial t} = f_p(h^i, h^{i-1}, p^i, p^{i-1}, p^{i+1}, T_W^i) \quad (29)$$

## 3 The DissDyn library structure

The library contains fluid-dynamic models for two-phase flow in heated pipes as well as models for components like tanks, phase separators, valves and pumps. Models are added to convert the direct normal irradiation into a heat flux on each absorber section.

### 3.1 Connector definitions

There are four different types of connectors currently defined in the library:

<u>MassFlow</u> }		
m_dot	[kg/s]	mass flow
h	[J/kg]	specific enthalpy
p	[Pa]	pressure
<u>AmbData</u> □		
t_amb	[°C]	ambient temp.
v_wind	[m/s]	wind speed
alpha_wind	[deg]	wind direction
<u>SolarIrr</u> ◇		
altitude	[deg]	altitude angle
azimuth	[deg]	azimuth angle
I_Dir	[W/m <sup>2</sup> ]	direct irradiation
I_Diff	[W/m <sup>2</sup> ]	diffuse irradiation
<u>ParabolIrr</u> ○		
cosphi(n)	[-]	cos( $\phi$ )
alpha_tr(n)	[deg]	track angle
I_Dir(n)	[W/m <sup>2</sup> ]	direct irradiation

This list is completed by the standard Modelica Signal connector. All fluid-dynamic components can be linked using the same connector `MassFlow`. This connector is based on the definitions in the *TechThermo* library developed at the institute [5]. The other three connectors are used to transfer information on solar irradiation and related quantities like incident angles.

### 3.2 Solar irradiation models

The transformation of direct irradiation coming from the sun into heat flux on the absorber tubes can be subdivided into three steps as illustrated in fig. 3. In the `SolarIrradiation` model altitude and azimuth angles of sun position are calculated based on the day of the year, time of day and geographical latitude and altitude. This component is prepared for the implementation of functions predicting the intensity of direct as well as diffuse solar irradiation throughout the day. At present, the magnitude of direct irradiation is specified by an external signal source.

In the second stage the irradiation finally reaching the individual collector is reduced by cloud coverage or by taking the collector out of focus. In the model `ParabolicField` the position and orientation of all collectors in the field is stored which is used to calculate the optimum track angle and the resulting incident angle for each collector individually. The magnitude of direct irradiation specified via the `SolarIrr` con-

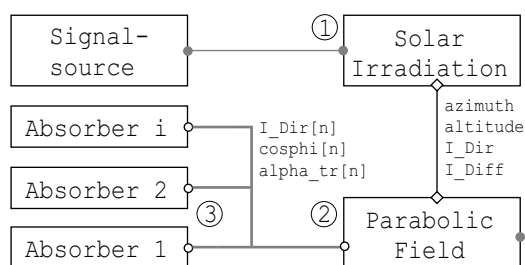


Figure 3: DissDyn-components used to model the path of solar energy from sun to absorber tubes

ector is reduced by a cloud coverage and focus information of the collector. The focus signal of each collector (range 0 to 1) can be read via the Modelica signal connector. Varying cloud coverage is represented using an one-dimensional cloud coverage signal that can be moved with arbitrary speed and direction over the collector field as shown in fig. 4

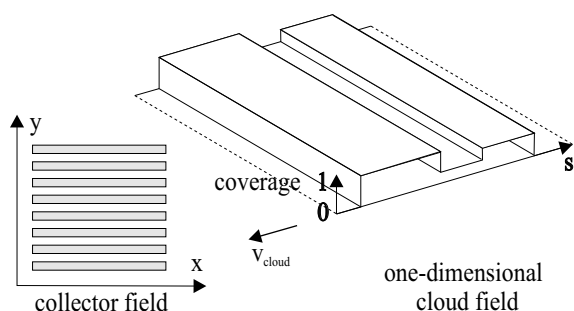


Figure 4: Cloud coverage

The final stage is the transformation of irradiation reaching the collector into the effective heat flux on the absorber tube. This task is implemented in the absorber model where efficiency data for the individual collectors are stored.

### 3.3 Absorber and pipe models

The model equations for two-phase flow in pipes presented in section 2 are used to construct models for simple pipe flow and for the flow in absorber pipes of parabolic trough collectors. The spatial discretization can be defined by the number  $n$  of axial elements along the pipe section. This is shown schematically in fig 5. For the computation of heat losses the ambient temperature is given via the AmbData-connector. The absorber models have another connector ParabolIrr by which information on actual irradiation, incident angle and theoretical track angle is provided. Since these values are constant along one collector each absorber model is intended to

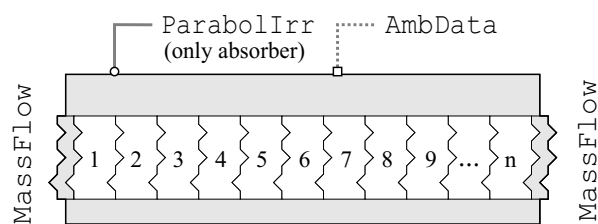


Figure 5: Structure of absorber and pipe model

represent one collector. A row of collectors is composed of a number of identical collectors and their interconnecting pipes. For convenience reasons a model collector\_Row is defined which holds a set of absorber and pipe models connected in series. All relevant geometrical parameters for the absorber and pipe model can be defined in this top level model. The irradiation and ambient data information is passed to each component as depicted in fig. 6.

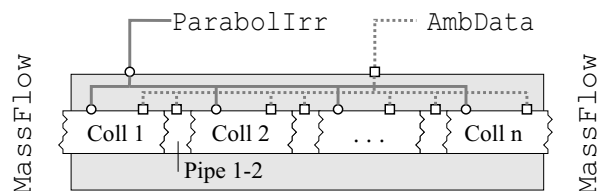


Figure 6: Collector\_Row model as a collection of absorber and pipe models

### 3.4 Fluid system components

The set of fluid models is completed by fluid system components like

- phase separator
- T-junction for flow combination and distribution
- control valve
- pump
- tank .

Except of the phase separator model all of these components are based on stationary conservation of mass and energy.

### 3.5 Control system components

To implement control functionality Modelica control models and specialized models are used. These models are linked by Modelica Signal connectors. Although these models can in principle be constructed

from Standard Modelica blocks new models are defined in order to have direct access to all relevant variables within one model.

## 4 Validation

The validation of the fluid dynamic models is done in two steps. First the simulation results with different spatial discretization are compared with analytical solutions available under special assumptions like constant pressure. Since these assumptions are not valid in the real system a direct comparison with measured data from the DISS test loop is needed in the second step.

### 4.1 Analytical models

Under some assumptions the set of conservation equations can be solved analytically by Laplace transformations [3], [4]. Using the same simplifications for the simulation the correct implementation and consistence of the simulation model can be checked.

Fig. 7 shows a comparison of transfer function in terms of amplitude and phase response for a 20 m absorber pipe section under two-phase conditions. For this comparison the reaction to a 1% step in irradiation with a spatial resolution of 1 element and 20 elements have been simulated. The corresponding trans-

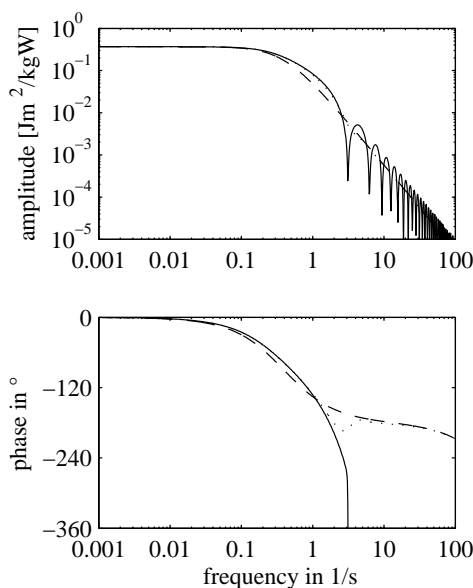


Figure 7: Transfer function of a 20 m two-phase absorber section: calculated with analytical model (-), simulated with discretization 1 element (- -), 10 elements (· · ·)

fer function is derived by Laplace transformation of the change in specific enthalpy at the outlet. While the simulation with just one element has large deviations from the analytical solution a much better agreement is obtained with high resolution of 20 elements indicating the consistence of the simulation model.

Comparison in the time domain plotted in fig. 8 shows that for high resolution nearly exact agreement is obtained. This means that the remaining deviations in

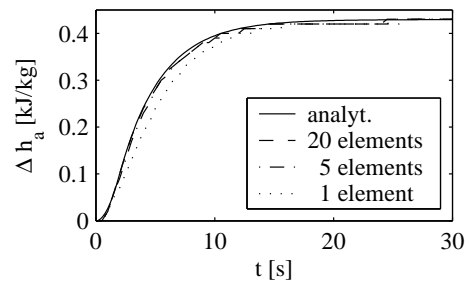


Figure 8: Step response to a 1% change in irradiation for a 20 m two-phase flow absorber

amplitude and phase angle at frequencies of more than 1/s are not serious for the system since the contribution of these frequencies is very small. Although the resolution with 20 elements gives nearly exact agreement the simulation with 5 elements is also very close to the analytical solution.

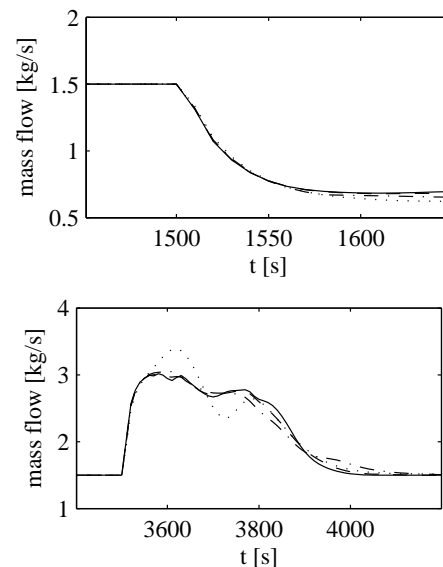


Figure 9: Simulated step response to changes in irradiation of  $-500 \text{ W/m}^2$  at  $t=1500 \text{ s}$  and  $+500 \text{ W/m}^2$  at  $t=3500 \text{ s}$ . 100 m evaporator section with resolution of 2.5 m (-), 10 m (- -), 33 m (- · -), 100 m (· · ·)

In Fig. 9 simulation results are shown for a 100 m evaporator section with large changes in irradiation.

These results are obtained without the simplifying assumption of constant pressure. The curves show that the result with the coarse resolution of 10 m is quite close to the one with fine resolution. Comparisons are performed for the preheating and superheating section as well giving similar results.

## 4.2 Comparison with measured data

Especially the assumption of constant pressure along the absorber is not fulfilled if multiple collectors are connected in series. The comparison with the analytical models on the basis of constant pressure is therefore not sufficient to validate the model. For this task a direct comparison with measured data from the DISS test loop is performed for several test days. As an example the reaction of the 500 m collector row (425 m preheater/evaporator, 75 m superheater) to irradiation fluctuations is shown in fig 10 in terms of inlet pressure, steam mass flow and steam temperature.

Though there is a small deviation in the absolute value of inlet pressure the dynamic behaviour is well predicted. Steam production and temperature are in good agreement which is also observed in the other test configurations. Both the check with analytical models and the direct comparison with measured data show that the model assumptions, especially the homogeneous equilibrium model are valid for this application.

## 5 Transient simulation of a collector loop

The simulation model is used to simulate the reaction of a collector loop to changes in irradiation. Since the dynamical behaviour is dominated by the amount of liquid evaporated, the 800 m boiler section alone is analyzed in the first step with the superheater replaced by an adequate pressure loss term. Constant boundary conditions for feed water flow and enthalpy as well as recirculation flow and enthalpy are imposed at the collector inlet. At the outlet of the field the pressure is fixed at 7 MPa.

Using measured irradiation data as input for the simulation is not useful when looking on general system behaviour. Moreover comparison of results with other researchers requires the same set of input data. This is avoided if a simple test signal is chosen which represents the main characteristics of real irradiation disturbances. In this work three single disturbances in series are used as a test signal, see fig. 11. This signal is defined only by the two parameters interval length  $\Delta t$  and

change of intensity  $\Delta I$ . The time constant of the collector system is closely linked to the residence time in the boiler section. Since the residence time for an 800 m boiler is approximately 700 s a series of short disturbances provokes an overlap of the system reactions. By using the test signal with three ramps the effects of this overlap can be studied. On the other hand, if long intervals are chosen a single isolated disturbance can be analyzed.

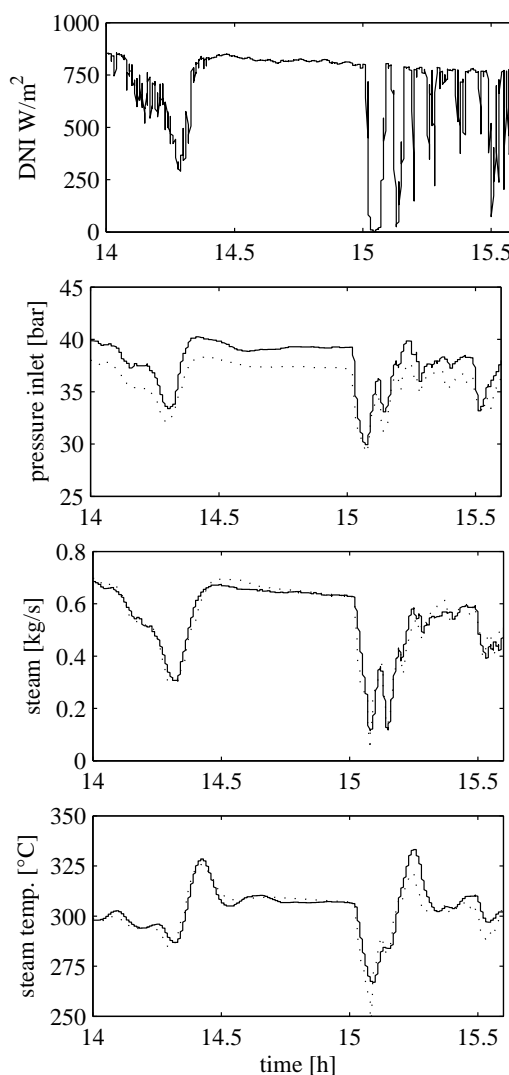


Figure 10: Measured (-) and simulated (···) DISS plant operation on June 26, 2001. Spatial Resolution 10 m.

### 5.1 Simultaneous disturbance on all collectors

Fig. 12 shows the simulation results in terms of steam and water mass flow at the exit of the evaporator section. Irradiation disturbances act simultaneously on

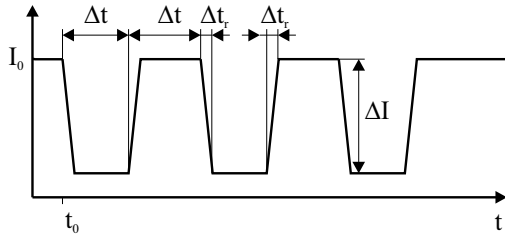


Figure 11: Test signal of three consecutive irradiation disturbances.

all 8 collectors of the boiler. Three studies with three different interval lengths are carried out. The intensity for short interval length is 100%, for long intervals only 70% in order to avoid reverse flow in the pipes. From the steam signal it can be seen that it takes about 700 s after the last disturbance to reach again stationary conditions. With a maximum interval length of 240 s all curves represent a superposition of individual reactions.

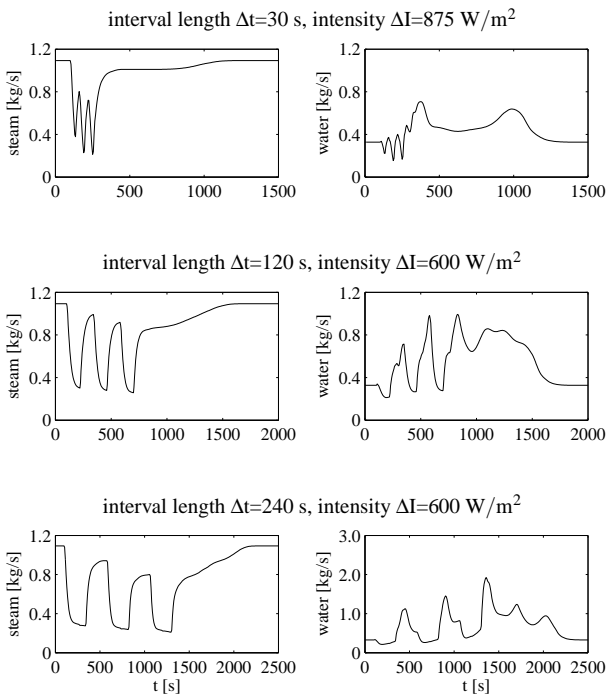


Figure 12: Reaction of the 800 m evaporator section to simultaneous irradiation disturbances on collectors 1-8 according to fig. 11. Plotted are steam and water mass flow at the exit of the evaporator. Feed water 1.2 kg/s, recirculation 0.25 kg/s, irradiation 875 W/m<sup>2</sup>, outlet pressure 7 MPa.

The water flow shows large peaks with the maxima located short time after the rising edge of the disturbance. Since constant feed flow is injected at the entrance of the collector water accumulates in the

system while irradiation is reduced. With increasing steam production this additional water is blown out and causes temporarily high liquid mass flux. In the  $\Delta t=30$  s case two peaks appear in the water mass flow signal. The first one immediately after irradiation increases and the second one with a delay of about 700 s just before stationary conditions are reached. While for short intervals ( $\Delta t=30$  s, 120 s) the second peaks of the three disturbances overlap and form one large peak the single peaks can be identified for longer interval length ( $\Delta t=240$  s). The maximum in liquid flow reached in this configuration is about 2.5 kg/s which is 8 times the nominal value. This results are very important to define the operating conditions for the layout of the compact field separator and the underlying drainage system.

### 5.2 Local disturbances

Small clouds can cause a local shading of just a number of collectors. Simulations are performed with assuming local shading of two collectors at a time. The same test signal is used as before. An additional configuration with a recirculation mass flow of 1.0 kg/s instead of 0.25 kg/s is simulated to estimate the impact of recirculation flow on the system dynamics.

Fig. 13 shows the results for a local shading of the pre-heating section (collectors 1 and 2). From the steam

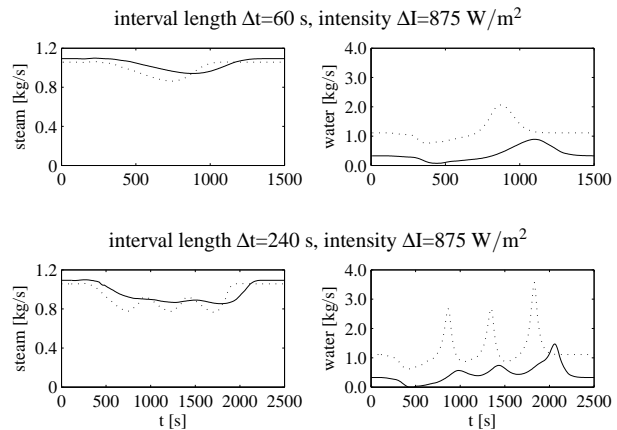


Figure 13: Reaction of 800 m evaporator section to local irradiation disturbance on collectors 1/2 according to fig. 11. Plotted are steam and water mass flow at the exit of the evaporator. Feed water 1.2 kg/s, recirculation 0.25 kg/s (-) / 1.0 kg/s (···), irradiation 875 W/m<sup>2</sup>, outlet pressure 7 MPa.

production it can be seen that the system reacts very slow. Since the fluid velocity is very small it takes a long time before the change in specific enthalpy leads

to a significant change in steam production. With increased recirculation flow the residence time in the preheating section gets smaller and reactions become faster and more distinct. This effect can be seen clearly in the water flow in the case  $\Delta t=240$  s. Although the integral value of liquid pushed out of the absorber is the same for both recirculation flows the temporal distribution differs. Since evaporation starts further downstream when collectors 1 and 2 are shaded liquid is stored in the system. This leads to a temporarily reduced liquid mass flow in the rest of the evaporator and, as a consequence, to a short period of dryout at  $t=500$  s. By increasing the recirculation flow the danger of superheating at the end of the evaporator is reduced. On the other hand much higher liquid peaks have to be accepted.

If the local shading is concentrated on collectors 4 and 5, see fig. 14, the reaction becomes faster and the peaks higher. At long intervals there is only weak

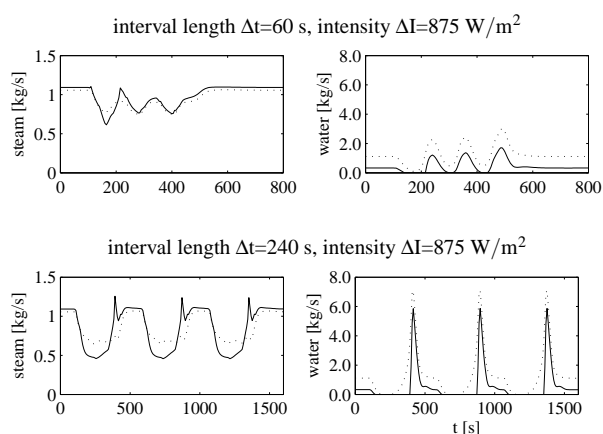


Figure 14: Reaction of 800 m evaporator section to local irradiation disturbance on collectors 4/5 according to fig. 11. Plotted are steam and water mass flow at the exit of the evaporator. Feed water 1.2 kg/s, recirculation 0.25 kg/s (-) / 1.0 kg/s ( $\cdot\cdot\cdot$ ), irradiation  $875 \text{ W/m}^2$ , outlet pressure 7 MPa.

overlapping of the single reactions. Compared with the shading of the pre-heater the reaction time now depends on the residence time in the two-phase region which is much shorter. Since the whole evaporator is nearly at the same temperature a change in steam production requires no heating or cooling of the absorber tube walls. The difference between small and high recirculation is small since recirculation mass flow has only minor impact on the average velocity. Compared to shading of collectors 1/2 the maximum liquid mass flow has nearly doubled and the dryout effect is much more critical. Even increasing the recirculation mass

flow can not avoid long periods of dryout.

Lokal Shading at the end of the evaporator in collectors 7/8, see fig. 15 is characterized by very small reaction time. The recirculation mass flow has no effect on the result. Water mass flow reaches its steady-state values very fast with nearly no dynamical overshooting.

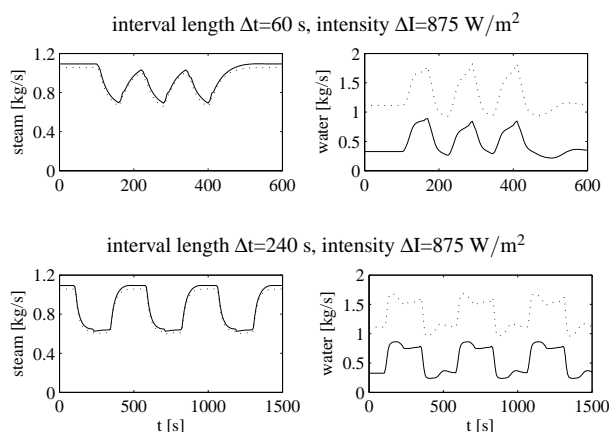


Figure 15: Reaction of 800 m evaporator section to local irradiation disturbance on collectors 7/8 according to fig. 11. Plotted are steam and water mass flow at the exit of evaporator. Feed water 1.2 kg/s, recirculation 0.25 kg/s (-) / 1.0 kg/s ( $\cdot\cdot\cdot$ ), irradiation  $875 \text{ W/m}^2$ , outlet pressure 7 MPa.

## 6 Combination with control system

A central task of the control system is to inject as much feed water as can be evaporated according to the actual irradiation. A standard feed-back control loop based on a liquid level control in the buffer tank reacts very slow to changes in irradiation. A much faster reaction is possible if measured irradiation is used to calculate the necessary feed flow. Another method is to measure the actual steam production and use this signal for the feed water pump. Due to model errors both approaches are not able to reach a specified set point in the buffer level so in any case an additional level controller is necessary. To analyze the potential of these forward control schemes simulations have been performed. Fig. 16 shows the results for a configuration of an uncontrolled system, a configuration with feed-forward control based on the irradiation measurement and a configuration with feed-forward control based on the steam production.

From the feed water signal the time lag between irradiation based and steam production based approach can

be seen. For liquid and gas mass flow at the evaporator outlet this lag has nearly no effect. The steam production gets more continuous with the feed-forward control. There is a significant reduction of maximum liquid peaks and as a consequence in buffer mass compared to the uncontrolled system. The reason is that

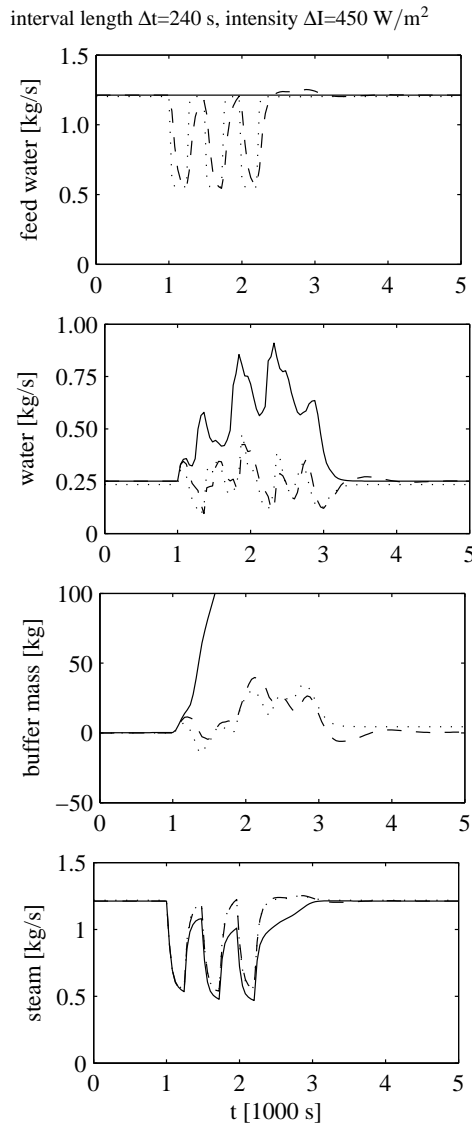


Figure 16: Comparison of uncontrolled (-) system with feed-forward control based on irradiation signal (···) and steam production (-.-). Recirculation 0.25 kg/s, DNI 900 W/m<sup>2</sup>.

less water accumulates in the pipes that has to be pushed out when irradiation again increases. In the presented disturbance configuration both feed-forward schemes give similar results. If local shading of the pre-heating section is used the irradiation based approach reacts much faster than steam production changes. This leads to a contradictory effect for the buffer level. As a preliminary result it can be stated

that the feed-forward control has shown high potential in reducing the necessary buffer size without significant negative side-effects.

## 7 Conclusions

A Modelica library for two-phase flow in parabolic trough collectors is developed and successfully validated against analytical models and experimental data. For the transient simulation of these complex system it is necessary to manually select the state variables and to transform the equations into explicit state space form. Only with this approach it is guaranteed that initialization and numerical integration are reliable without losing much of the flexibility the Modelica language offers. The library is used at the institute to simulate the reaction of parabolic trough collector loops with direct steam generation to fluctuations in solar irradiation.

## References

- [1] ECK M., STEINMANN W.-D. Direct solar steam generation in parabolic troughs: First results of the DISS project. In: *Journal of Solar Energy Engineering* (124), pp. 134-139, 2002.
- [2] MÜLLER-STEINHAGEN H., HECK K. A simple friction pressure drop correlation for two-phase flow in pipes. In: *Chem. Eng. Process.*(20), pp. 297-308, 1986.
- [3] PROFOS P. *Die Regelung von Dampfanlagen*. Berlin, Springer, 1962.
- [4] ECK M. *Die Dynamik der solaren Direktverdampfung und Überhitzung in Parabolrinnenkollektoren*. VDI-Fortschrittsberichte, Reihe 6, Nr. 464. Düsseldorf: VDI-Verlag, 2001.
- [5] STEINMANN W.D., ZUNFT S. TechThermo - A library for Modelica Applications in Technical Thermodynamics. In: *Proceedings of the 2nd International Modelica Conference 2002*, Oberpfaffenhofen, Germany, Modelica Association, 18-19 March 2002.